The Contribution of Shear to the Evolution of a Convective Boundary Layer

DAVID PINO

Institut d'Estudis Espacials de Catalunya, and Departament de Física Aplicada, Universitat Politècnica de Catalunya, Barcelona, Spain

JORDI VILÀ-GUERAU DE ARELLANO

Meteorology and Air Quality Group, Wageningen University, Wageningen, Netherlands

PETER G. DUYNKERKE*

Institute for Marine and Atmospheric Research, Utrecht University, Utrecht, Netherlands

(Manuscript received 21 February 2002, in final form 11 February 2003)

ABSTRACT

The role of shear in the development and maintenance of a convective boundary layer is studied by means of observations and large eddy simulations (LESs). Particular emphasis is given to the growth of the boundary layer and to the way in which this growth is affected by surface fluxes of heat and moisture and entrainment fluxes. This paper analyzes the processes that drive the latter mechanism, which accounts for approximately 30% of the growth of the mixing layer. Typically, it is found that under pure convective conditions, without shear, the entrainment buoyancy flux at the inversion is about −20% of the surface buoyancy flux. This value is widely used for entrainment rate closures in general circulation models.

The data collected during the Atmospheric Radiation Measurement campaign allow one to introduce realistic vertical profiles and surface fluxes into the LES runs and to compare the simulation results with the observed evolution of the boundary layer height during a convective situation with high entrainment rates and high geostrophic winds. The analysis of the turbulent kinetic energy (TKE) budget shows that the inclusion of geostrophic winds, which produce shear at the surface and in the entrainment zone, modifies the vertical profile of the various terms in the TKE budget. As a consequence, the entrainment flux is enhanced, resulting in increased growth of the boundary layer. The numerical experiments and the observations enable one to validate the efficiency of earlier representations, based on the TKE equation, which describe the evolution of the ratio between entrainment and surface buoyancy fluxes. The proposed parameterization for the entrainment and surface buoyancy flux ratio (β), which includes the main buoyancy and shear contributions, is in good agreement with the LES results. Some aspects of the parameterization of β, for instance, the absence of entrainment flux and its behavior during the transition between convective to neutral conditions, are discussed.

1. Introduction

The development and maintenance of a well-mixed boundary layer have a direct influence on many atmospheric phenomena, such as cloud formation or pollutant distribution. The growth of this convective boundary layer (CBL) is driven by both surface fluxes of heat and moisture and by the entrainment of dry and more buoyant air from the free atmosphere. Wind shear at the surface and at the inversion layer can modify the physics of these processes. The ratio between these two forces (buoyancy and shear) can substantially affect the depth of the mixed layer, the CBL characteristics, and the turbulence statistics (Arya and Wyngaard 1975; Schimdt and Schumann 1989; Sorbjan 2001; Fedorovich et al. 2001a,b). When both shear and buoyancy are important, the structure of the CBL flow is found to differ from the structure of either a purely mechanical boundary layer or a convective boundary layer (Sykes and Henn 1989; Moeng and Sullivan 1994; Khanna and Brasseur 1998). Moreover, observations have shown that in a CBL where both forces are present, the convection pattern is in the form of horizontal rolls (LeMone 1973; Christian and Wakimoto 1989).

From 1970 onward many researchers (Tennekes 1973; Stull 1976a; Zeman and Tennekes 1977; Tennekes and Driedonks 1981; Driedonks and Tennekes 1984; Fedorovich 1995) have concentrated on studying the evolution of the ratio of buoyancy fluxes at the inversion

*Deceased.

Corresponding author address: David Pino, Institut d'Estudis Espacials de Catalunya (IEEC/CSIC), Edif. Nexus, Gran Capità 2-4, 08034 Barcelona, Spain.
E-mail: pino@ieec.fcr.es

TABLE 1. Locations of the radiosondes and surface sites used in this study.

Site	Lat (°)	Lon (°)	Elev (m)
	Radiosonde sites		
C1	36.605	−97.485	315
B1	38.305	−97.301	447
B4	36.071	−99.218	622
B5	35.688	−95.856	217
B6	34.969	−97.415	345
	Surface sites		
C1	36.605	−97.485	318
E4	37.953	−98.329	513
E9	37.133	−97.266	386
E12	36.841	−96.427	331
E15	36.431	−98.284	418

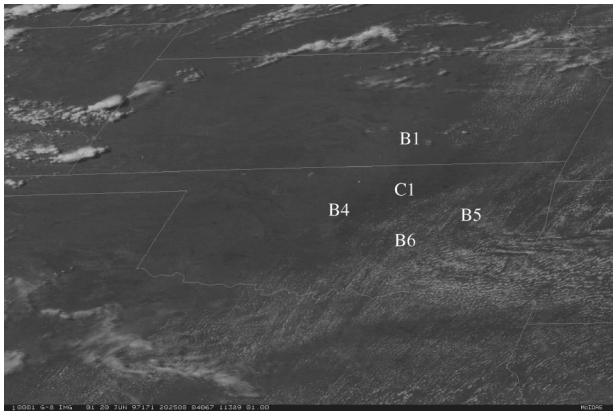

FIG. 1. *GOES-8* visible image at 2025 UTC 20 Jun 1997 at the SGP site. The coordinates in the bottom left and top right corners of the image are approximately (32°N, 104°W) and (42°N, 94°W). The approximate location of the various radiosonde facilities used in the study is also shown.

level and at the surface, $\beta = -\overline{w\theta_v}\,|_h/\overline{w\theta_v}\,|_0$. The main goal of these studies was to develop a suitable parameterization for the entrainment flux. From the turbulent kinetic energy (TKE) budget, it is possible to obtain an expression that depends only on variables that can be obtained from observations and can be compared with these observations (Artaz and André 1980; Dubosclard 1980; Driedonks 1982b; Culf 1992; Betts and Ball 1994). By comparing different models for the ratio of buoyancy fluxes at ground level and at the inversion level, or for the boundary layer depth with observations, the authors of some of these studies pointed to the need for taking shear into account in the parameterization of the entrainment coefficient.

On the basis of observations and large eddy simulations (LESs), we discuss the role played by shear at the surface and at the inversion level and its influence on the entrainment flux. The study stems from a specific situation that occurred on 20 June 1997 at the Southern Great Plains (SGP) Atmospheric Radiation Measurements (ARM) site (Barr and Sisterson 2000), where a convective boundary layer with high entrainment rates (related to the time derivative of the mixed-layer depth) and increasingly strong horizontal winds was observed. Three simulations were performed by means of LES, and the results were compared with the evolution of the observed CBL. All the simulations are based on the same realistic initial vertical profiles, except for the mean winds and surface heat fluxes obtained from the ARM sites. Briefly, an experimental case with pure buoyancy-driven CBL and two intermediate CBLs driven by both shear and buoyancy forces were set up. In these intermediate CBLs, initial wind shear is prescribed from the observed values in the one case, and in the other case it is restricted to the surface level. The vertical profiles of potential temperature, specific humidity, and mean winds are compared with the observed profiles. The evolution of the mixed-layer depth is also studied.

From the three simulations, we have analyzed the different contributions of the TKE budget at the entrainment zone. Historically, two key parameters have been used for studying the entrainment processes: the entrainment rate (Culf 1992) or the ratio between entrainment buoyancy flux and surface buoyancy flux β (Dubosclard 1980). However, both variables are related (Garratt 1992). Here, we study the buoyancy flux ratio by means of LES and evaluate and extend a parameterization of flux ratio previously proposed by Driedonks (1982b). The β parameterization includes the main physical processes that drive the buoyancy flux at the entrainment zone. Because of its simplicity, it can easily be implemented in general circulation models (GCMs). The expression is related to the entrainment law $E \propto \mathrm{Ri}^{-1}$, where E is the entrainment rate defined as $E = w_*^{-1}dh/dt$, $w_* = (gh\overline{w\theta_v}\,|_0/\overline{\theta_v})^{1/3}$ and $\mathrm{Ri} = h\Delta\theta_v w_*^{-2}$ is a Richardson number (Betts 1973; Carson 1973; Tennekes 1973). In these expressions, h is the mixed-layer depth defined as the height of the minimum buoyancy flux, $\overline{\theta_v}$ is the mean virtual potential temperature in the mixed layer, and g is the acceleration due to gravity. In this research, the parameterization for the buoyancy flux ratio is successfully tested by comparing them with the simulation results.

2. Observational variables and numerical setup

a. Observations

At the SGP site of the ARM program, located in Oklahoma and Kansas, various types of atmospheric measurements are continuously monitored by in situ observations and remote sensing (see Table 1 and Fig. 1 for the locations of the facilities referred to in this paper). The vertical profiles of potential temperature, specific humidity, and horizontal winds were measured by means of five different radiosondes, which were launched every 3 h from each of the sites listed in Table 1. At site C1 (Central Facility), wind profiler measurements were taken to determine the depth of the atmospheric boundary layer (ABL) and the vertical wind

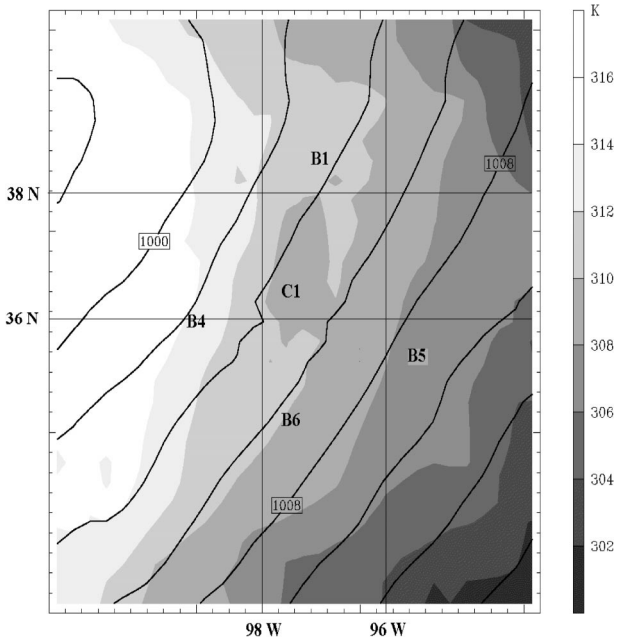

FIG. 2. Surface pressure (solid lines) and temperature (shaded contour) calculated by the MM5 model at 1800 UTC. The locations of the different radiosonde facilities used in the study are also shown.

profile. In addition, other relevant variables for the evolution of the ABL, such as the surface sensible and latent fluxes, were estimated from observations (see Table 1) using the energy balance Bowen ratio method.

A CBL with high entrainment rates was observed on 20 June 1997. During the day, clear skies were reported at all the sites except B5 (see Fig. 1). The synoptic situation was characterized by a low-level pressure system located west of the studied area, which caused south-southwesterly winds and a decrease in the ground temperature toward the east. Figure 2 shows the surface pressure and temperature calculated from the fifth generation Pennsylvania State University–National Center for Atmospheric Research Mesoscale Model (PSU–NCAR MM5; Dudhia 1993) at 1800 UTC (LST = UTC − 6). The radiosonde locations of the various facilities used in this study have been added to this figure.

b. Numerical setup

To simulate the evolution of the ABL in the course of 20 June 1997, and to study the importance of the entrainment fluxes in this evolution, we performed three different runs of the LES model described in Cuijpers and Duynkerke (1993) and recently modified by Cuijpers and Holtslag (1998). In the three simulations, all the initial and boundary conditions are identical except for the initial wind profile. The first case is defined as a boundary layer driven only by pure surface buoyancy, without geostrophic winds, namely, B (buoyancy). The second and third cases, where geostrophic winds are introduced, represent flows driven by both shear and buoyancy. In the former case [buoyancy-geostrophic (BG)], the initial geostrophic wind is constant with height and the shear occurs only at the surface. In the latter case, the initial wind profile corresponds approximately to the winds observed during the day. In this simulation the initial geostrophic shear also occurs near the inversion [buoyancy-geostrophic-sheared (BGS)].

As mentioned above, the same surface fluxes are considered in the three simulations. The maximum values of the surface sensible and latent heat fluxes for the simulations are obtained by adjusting a sinusoidal function to the average flux of the measurements of each facility presented in Table 1. In this way, we find the maximum values of the sensible and latent heat flux to be SH = 120 W m^{-2} and LE = 440 W m^{-2}. Figure 3 shows the diurnal variation on 20 June 1997 of surface heat fluxes measured by each facility and the surface sensible and latent heat fluxes used in the simulations (Figs. 3c and 3d). During the day, typical diurnal evolution of the various terms of the energy budget for a vegetated land surface at midlatitudes was observed at all surface sites. In this situation, $-F_{\text{net}}$ is positive because more radiation enters the ABL downward than leaves it upward; SH and LE are positive because heat and moisture are transported upward; and finally, G is negative because heat is conducted downward into the ground.

A 6.4 km × 6.4 km × 3 km domain with grid spacing $\Delta x = \Delta y = 100$ m and $\Delta z = 50$ m is defined. The total simulation time was 11 h starting from 1300 UTC, that is, the entire daily evolution, and the model output was recorded every 5 min. The radiosonde at 1430 UTC is used as the initial vertical profile of potential temperature ($\overline{\theta}$) and specific humidity ($\overline{q}$). The initial mean potential temperature (specific humidity) profile for all the simulations is 306 K (15.6 g kg^{-1}) below 625 m; it increases by 6 K (decreases by 9.8 g kg^{-1}) up to 825 m, and increases until it reaches 317.8 K at 3 km (above this point, specific humidity has a constant value of 5.8 g kg^{-1}).

During the day in question, the CBL development was influenced by shear at the surface and in the entrainment zone. Two different initial vertical profiles for the horizontal winds are prescribed (BG and BGS simulations). The values obtained from the radiosondes and the wind profiler indicate that there were high winds the whole day. From the observational data, the geostrophic wind speed above 1000 m was $U_g = V_g = 10$ m s^{-1}. Below this level, and in spite of the scatter of the data, $U_g = 10$ m s^{-1} and $V_g = 17$ m s^{-1} are reasonable values. These wind profiles are used as the initial wind vertical profiles in the BGS simulation. In order to clarify the role played by surface shear in the evolution and maintenance of the ABL, an additional simulation (the BG simulation) was performed with $U_g = V_g = 10$ m s^{-1} in the entire simulated domain. All these initial vertical profiles are shown in section 3.

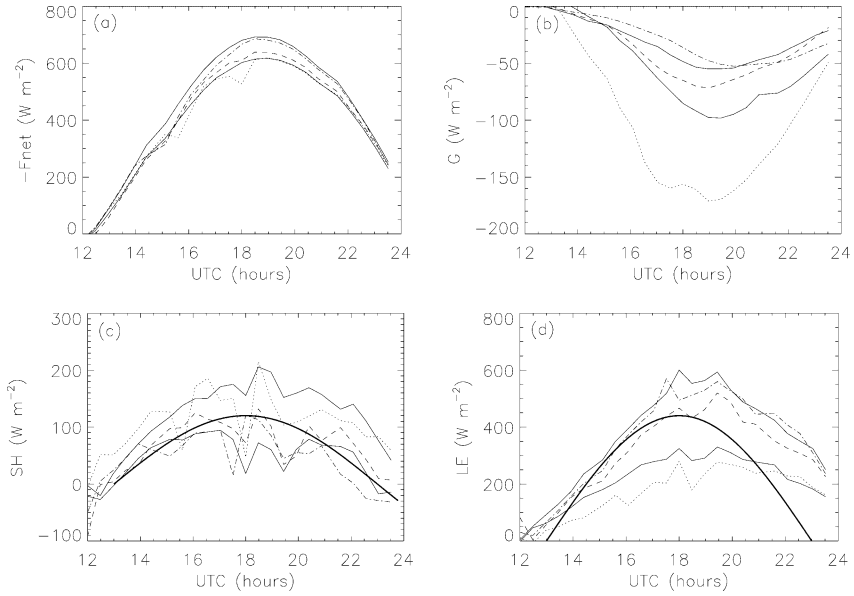

FIG. 3. Surface fluxes obtained by each facility (C1, E4, E9, E12, E15) by means of the Bowen ratio method. (a) Net radiation, (b) heat into the ground, (c) sensible heat flux, and (d) latent heat flux. In (c) and (d) the thick solid line shows the sensible and latent heat fluxes prescribed in the simulations.

3. Results

a. Potential temperature and specific humidity

Figure 4 compares the vertical profiles of the potential temperature and specific humidity observed by the radiosondes (symbols) and obtained with the B, BG, and BGS simulations (different type of lines) for three different moments in the day (from top to bottom, 1730, 2030, and 2330 UTC, corresponding to 1130, 1430, and 1730 LST, respectively). In order to compare with the measured vertical profiles at 1730, 2030, and 2330 UTC, we have selected the profiles calculated by averaging the simulation results between 4–5, 7–8, and 10–11 h, respectively since our simulation started at 1300 UTC. The initial vertical profiles for $\overline{\theta}$ and $\overline{q}$ are also plotted in all the figures (dotted lines). In these figures, we decided to use the height above sea level to show that similar temperature and moisture jumps are observed at similar height above all the sites. Notice that, in general, all the simulations correspond reasonably well to the evolution and the vertical distribution of the CBL on a clear day. Our primary goal is not to compare each observed profile with the LES results, but to show that the LES could simulate the main characteristics of the observed convective boundary layer when the shear contribution could play a key role. The calculated profiles follow rather well the vertical profile evolution of the temperature and moisture observations. In spite of the scatter of the observations, the BGS case fits slightly better to the observations, in particular with the radiosonde observations taken at the main site C1 (crosses) at 2030 and 2330 UTC. In general, the B simulation tends to calculate a lower inversion height. In both simulations BG and BGS, due to the larger entrainment fluxes, we obtained deeper boundary layers.

b. Mean winds

Due to the scatter of the wind profiler data and the radiosonde observations for the u and v components of the wind, only the observations around the central part of the day (between 1900 and 2100 UTC) are considered. Figure 5 shows the mean winds obtained by the various observational methods and the results of the simulation BGS around 2030 UTC. As can be observed, there is a good agreement between the radiosonde at 2030 UTC and the LES output averaged between 7 and 8 h of simulation. Both profiles fit approximately in the middle of the data provided by the wind profiler located at C1. This time, the values obtained for the velocity scales of BGS simulation are $u_* = [(\overline{uw}|_0)^2 + (\overline{vw}|_0)^2]^{1/4}$ equal to 0.69 m s^{-1} and w_* equal to 1.7 m s^{-1}. The ratio between these velocity scales is the relevant parameter in sheared convection. Some controversy exists regarding the critical value for the formation of the roll vortices. LeMone (1973) have observed horizontal roll vortices in moderately convective boundary layers ($u_*/w_* \gtrsim 0.34$). While Sykes and Henn (1989) with their LES suggested the ratio $u_*/w_* > 0.35$, whereas Moeng and Sullivan (1994) only found these characteristic phenomena for values u_*/w_* larger than 0.65. Khanna and Brasseur (1998) by means of LES obtained clear roll vortex structures for values u_*/w_* equal to 0.37 and 0.5. In our case, for the BGS simulation, rolls are

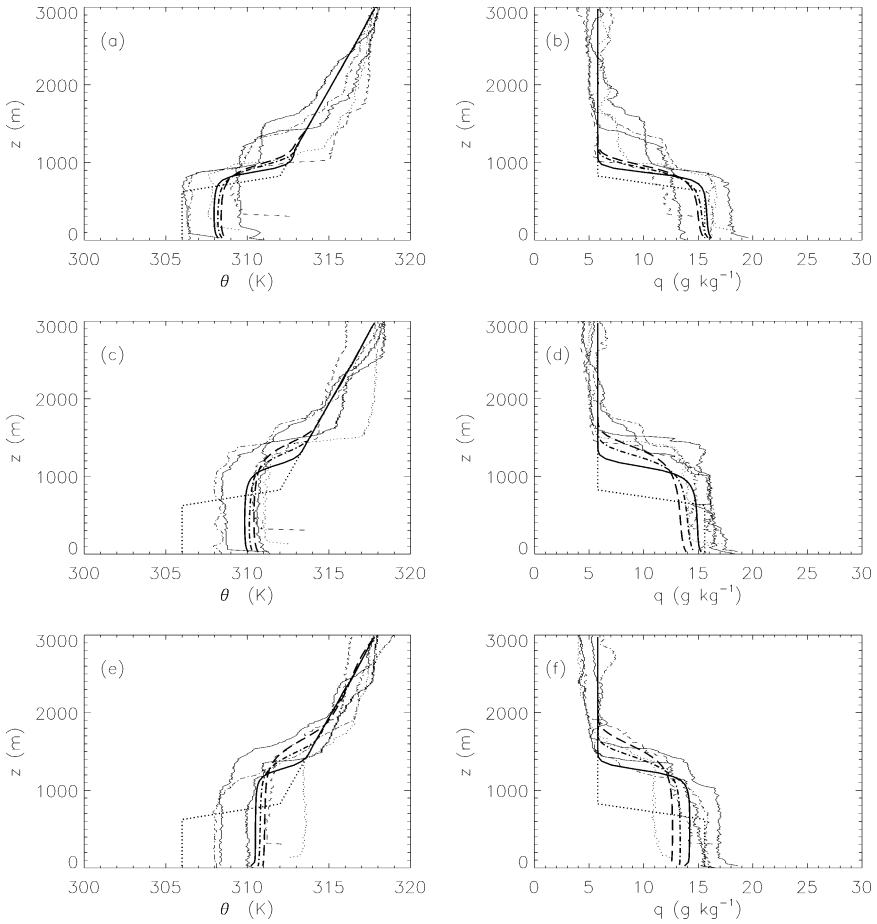

FIG. 4. (left) Potential temperature and (right) specific humidity vertical profiles obtained at the radiosonde sites (symbols) at (top) 1730 UTC, (middle) 2030 UTC, and (bottom) 2330 UTC: C1, B1, B4, B5, B6. The lines represent the initial vertical profiles (dotted line), and the vertical profiles obtained by the B simulation (solid line), the BG simulation (dashed–dotted line), and the BGS simulation (dashed line). To compare LES vertical profiles and the different radiosondes, the temporal integration of the LES output between 4 and 5, 7 and 8, and 10 and 11 h is considered. All the radiosondes were shifted in order to obtain approximately the potential temperature of C1 above the inversion layer at 1730 UTC. B1, B4, B5, and B6 are shifted by -1, -2, $+2$, and $+1$ K, respectively. Note that the observed vertical profiles start at different heights because no modification has been made to the elevation of the radiosonde sites.

formed at 1730 and 2030 UTC for the following values of $u_*/w_* = 0.40, 0.45$. These values are in close agreement with the observed values at the only site where have surface and upper-air observations (C1): $u_*/w_* = 0.32$ at 1730 UTC and 0.41 at 2030 UTC. Figure 6 depicts a horizontal cross section of the instantaneous specific humidity field after 4 h of simulation (1700 UTC) at $z/h = 0.5$, where h is the height of the minimum buoyancy flux, for the B and the BGS simulations. At this time $u_*/w_* \approx 0.4$ for the BGS case. The BGS simulation reveals a two-dimensional roll pattern (Fig. 6b). We have some experimental evidence of the existence of these structures by looking at the satellite picture, which shows (right-hand side of Fig. 1) the presence of cumulus cloud streets aligned with the mean flow direction (Moeng and Sullivan 1994; Khanna and Brasseur 1998). This structure does not appear in the pure buoyancy flow of simulation B. In that case, the flow is characterized solely by convective cells, as seen in Fig. 6a.

c. *Turbulence kinetic energy budget*

Clearly, then, shear introduces large modifications into the mean properties of the boundary layer. It is therefore necessary to analyze how the shear modifies a fundamental variable for the boundary layer evolution: the turbulent kinetic energy. Under horizontally homogeneous conditions and without subsidence, the turbulence kinetic energy budget can be expressed as

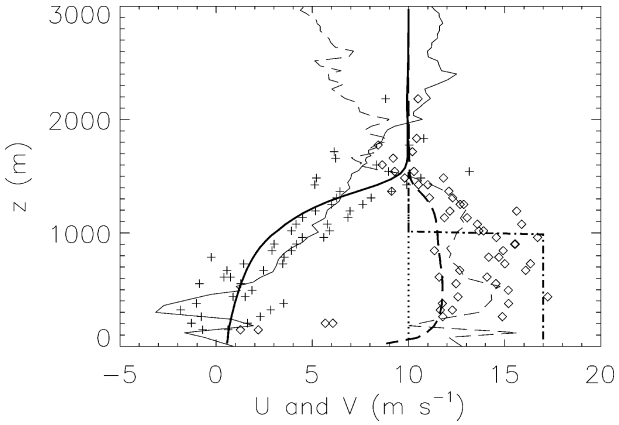

FIG. 5. Vertical profiles of mean winds. The radiosonde profiles obtained at C1 at 2030 UTC [U (solid line), V (dashed line)] are shown with thin lines. The thick lines represent velocities integrated between 7 and 8 h [U (solid line), V (dashed line)], and the initial profile of the BGS simulation [U (dotted line), V (dashed-dotted line)]. Crosses and diamonds are, respectively, U and V velocity measured between 1900 and 2100 UTC by the wind profiler located at C1.

$$\frac{\partial \overline{e}}{\partial t} = -\left[\overline{uw}\frac{\partial U}{\partial z} + \overline{vw}\frac{\partial V}{\partial z}\right] + \frac{g}{\overline{\theta_v}}\overline{w\theta_v} - \frac{\partial \overline{we}}{\partial z} - \frac{1}{\overline{\rho_0}}\frac{\partial \overline{wp}}{\partial z} - \epsilon, \quad (1)$$

where (u, v, w) are the fluctuating velocity components; U, V are the horizontal components of the mean wind; p is the pressure; $\overline{\rho_0}$ is a reference density; $\overline{\theta_v}$ is a reference virtual potential temperature; $\overline{e} = 0.5(\overline{u^2} + \overline{v^2} + \overline{w^2})$ is the time average of the turbulent kinetic energy (Stull 1988); and

$$\epsilon = -\nu\left[\overline{u\left(\frac{\partial^2 u}{\partial z^2}\right)} + \overline{v\left(\frac{\partial^2 v}{\partial z^2}\right)}\right] \quad (2)$$

is the molecular dissipation of TKE. The term on the left-hand side represents the tendency of TKE (TE), and the terms on the right-hand side are the shear production (S), the buoyancy production (B), the turbulent transport (T), the pressure transport (P), and the molecular dissipation term (D). The first two terms on the right-hand side are sources, the next two only redistribute the TKE vertically and the last one is a sink. Usually, terms T and P are considered together as the convergence of the turbulence kinetic energy flux (Driedonks 1982b).

The total TKE budget for the B, BG, and BGS simulations after 8 h of simulation (2100 UTC) is shown in Fig. 7. In the TKE budget of the B simulation (Fig. 7a), the primary source term is buoyancy. In this case, as the shear term is zero, under quasi-steady-state conditions there is a balance between the sum of the dissipation and buoyancy terms and the pressure and transport contributions. With regard to the BG TKE budget (Fig. 7b), the inclusion of shear at the surface affects the other terms of the budget. The buoyancy term decreases with respect to simulation B near the surface and at the inversion level, but it does not change in the middle of the CBL. In order to balance the shear production term, the dissipation term increases its value, and is nearly uniform with height except very close to the surface, and the pressure term becomes a consumption term at the inversion. Note that, in this case, although initially wind shear is only prescribed at the surface, a shear contribution develops at the inversion level. However, wind shear remains very small in the middle of the CBL. This is because surface fluxes generate large thermals that can effectively mix the mean winds in the middle of the CBL (see Fig. 5) reducing $\partial U/\partial z$, and hence reducing the shear production (Moeng and Sullivan 1994). According to simulation BGS (Fig. 7c), the shear at the inversion level decreases the buoyancy term (increases its absolute value) at this level with respect to the BG simulation and, as a result, increases the contribution of the dissipation term in order to balance the shear term. Pressure and transport terms change by compensating each other. With regard to the entrainment flux, one should notice the importance of the shear term as a production term at the inversion. This term is larger in the BGS case than in the BG simulation. Consequently, we can expect an enhancement of this flux. It is therefore advisable to include the contribution of shear in a parameterization of the entrainment flux (see section 4).

d. Buoyancy flux

To demonstrate the differences between the entrainment fluxes in the various simulations, we show in Fig. 8 the buoyancy flux (total and subgrid contributions) averaged between 7 and 8 h and normalized by the surface buoyancy flux for the three cases performed. As expected in a clear-day situation, in all the simulations the buoyancy flux decreases linearly with height; it has a large positive value near the surface and becomes negative near the top of the mixed layer (Stull 1988). The negative value of the buoyancy flux near the mixed-layer top is associated with the entrainment of warmer and drier air from the free atmosphere into the mixed layer. As shown, higher values at greater heights are found for the entrainment fluxes with the BG simulation than with the B simulation. It is therefore clear that surface shear enhances the entrainment flux. This flux will increase with the extra shear contribution at the inversion (Garratt 1992). This is shown in Fig. 8 by observing the buoyancy flux in the BGS simulation. Notice also that shear increases the contribution of the small scales of the turbulent kinetic energy and, in consequence, the subgrid fluxes become larger at the entrainment zone. As reported in previous studies (Tennekes 1973; Fairall 1984), Fig. 8 also shows that wind shear in the boundary layer enhances the growth of the mixing layer. This conclusion is connected with the be-

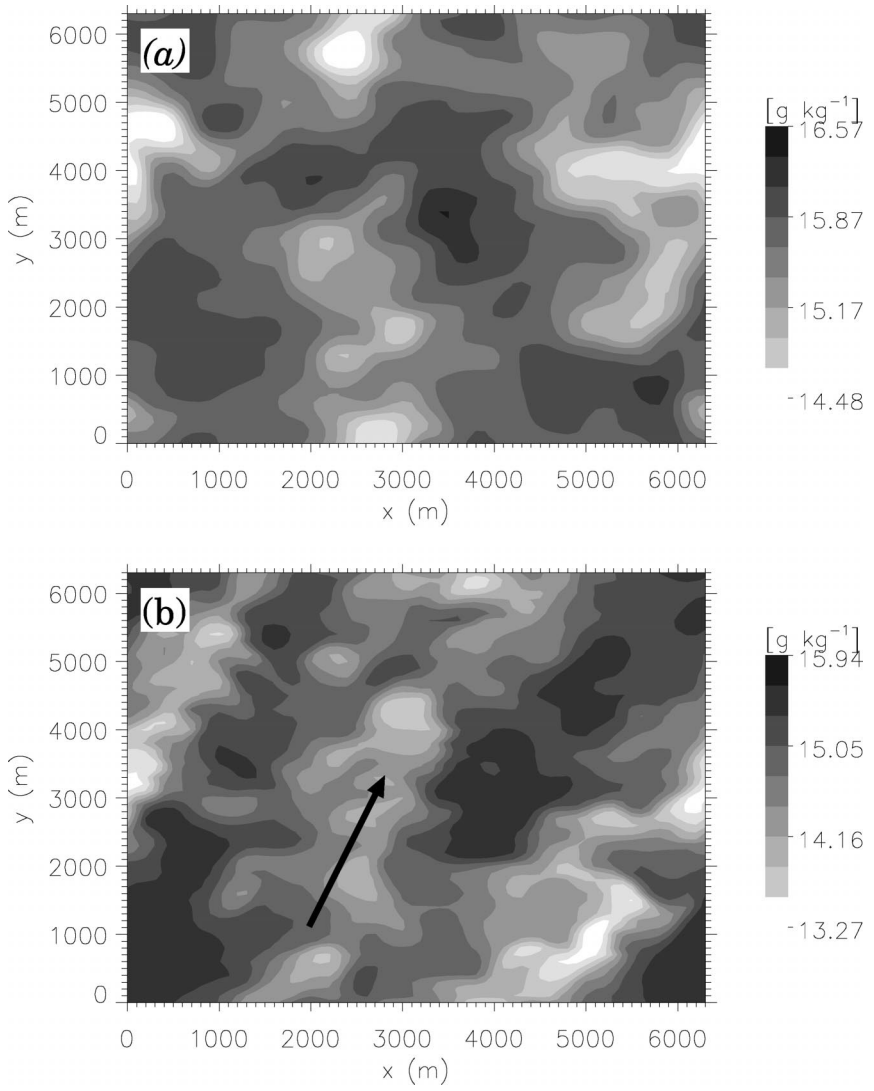

FIG. 6. Contours of the specific humidity in the x–y plane at $z/h = 0.5$ after 4 h of simulation (1700 UTC) for the (a) B and the (b) BGS simulations. The whole domain covers about $6.5h \times 6.5h$. In (b), the arrow marks the wind direction at this time.

havior of the TKE budget presented in Fig. 7. Therefore, from our simulations we can conclude that shear at the inversion level enhances the turbulence at this level (see Fig. 7c).

e. Mixed-layer depth

Figure 9 shows the evolution of the mixed-layer depth (MLD) on 20 June 1997 as inferred from the radiosonde observations (symbols). Although some authors (e.g., Stull 1988) have expressed reservations about deriving the depth of the mixed layer from the ascent of a single radiosonde, the scatter of the direct measurements of the MLD by the wind profiler forces us to use the radiosonde data. Driedonks (1982b) calculated that the error made by obtaining the MLD from an individual radiosonde was as much as ± 100 m. It is important to notice that Fig. 9 shows only the evolution of the mixed-layer depth up to 2100 UTC. This was the time at which the turbulence generated by convection began to decay due to the decrease in the sensible heat flux (see Fig. 3). As was observed, all the facilities shown in Fig. 1 give at the different times approximately the same values for MLD, except at C1 at 1730 UTC. Also shown (lines) are the time evolution of the height of minimum buoyancy flux h and the height h_s at which the concentration of a bottom-up passive scalar reaches a threshold value (Garratt 1992; Driedonks and Tennekes 1984; Bretherton et al. 1999) obtained by the three simulations performed. Specifically, in our case the initial concentration of the inert scalar is set to 0 kg kg^{-1}, a constant surface flux of 0.1 kg kg^{-1} m s^{-1} is prescribed and h_s

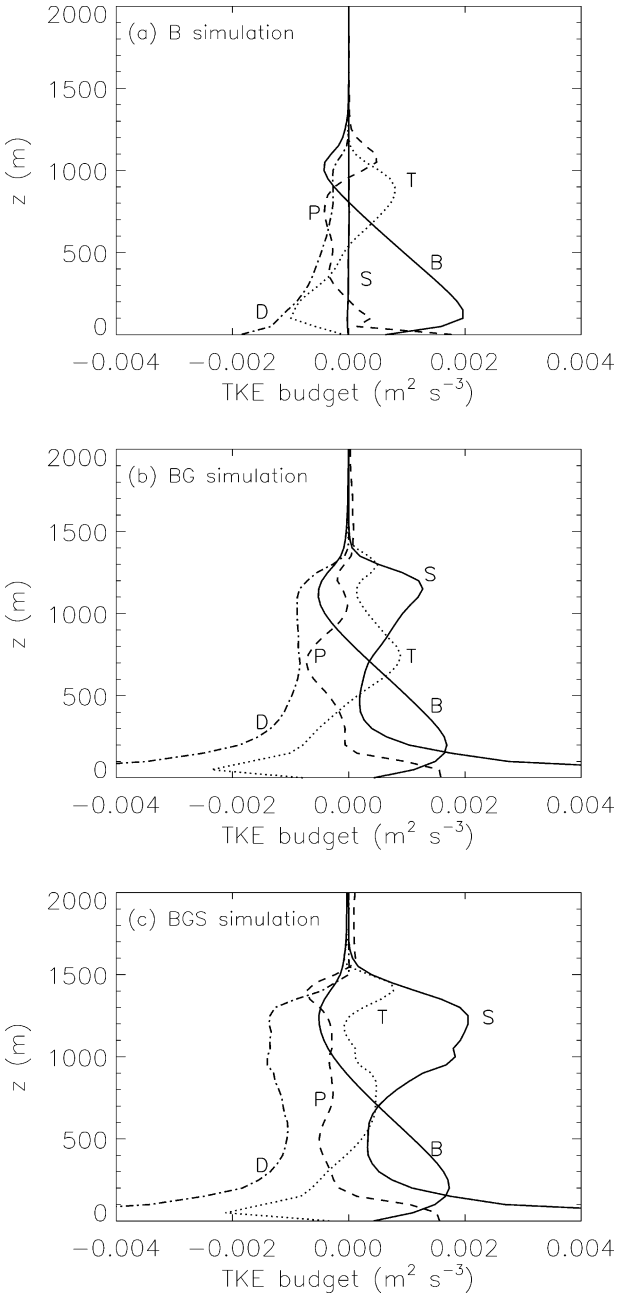

FIG. 7. Vertical distributions of the various terms (buoyancy, dissipation, pressure, transport, and shear) in the TKE budget for (a) B, (b) BG, and (c) BGS simulations averaged between 7 and 8 h of simulation (2000–2100 UTC).

is considered as the height at which the scalar concentration is 0.5 kg kg^{-1}. The figure shows consistency between the two methods, and in the three simulations performed $h_s > h$. As the vertical profiles of Fig. 4 also show, BGS simulation produces, close to the maximum values for sensible and latent heat flux, that is, between 1800 and 2000 UTC, the largest values of h and h_s. These values also agree better with the observed MLD. On the other hand, the pure buoyancy CBL of simulation

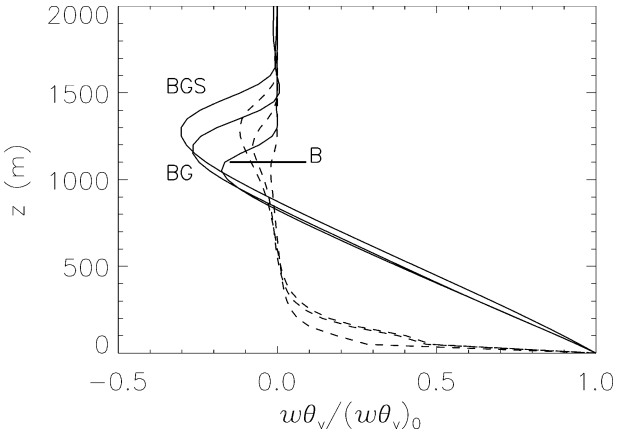

FIG. 8. Vertical profile of the total buoyancy flux normalized by its surface value (solid lines) time averaged between 7 and 8 h of simulation for B, BG, and BGS simulations (solid lines). The normalized subgrid-scale contributions for each simulation (dotted lines) are also shown.

B clearly underestimates the observed MLD evolution. When the shear occurs only at the surface level, the BG simulation reproduces an intermediate situation.

4. Parameterization of the entrainment flux

General circulation models (GCMs) are unable to calculate the entrainment flux and boundary layer depth explicitly. They parameterize it as a function of known quantities, such as the surface buoyancy flux or the friction velocity. These parameterizations usually do not include some of the physical aspects that can influence entrainment flux, such as, wind shear at the inversion zone. The parameterization for the entrainment flux con-

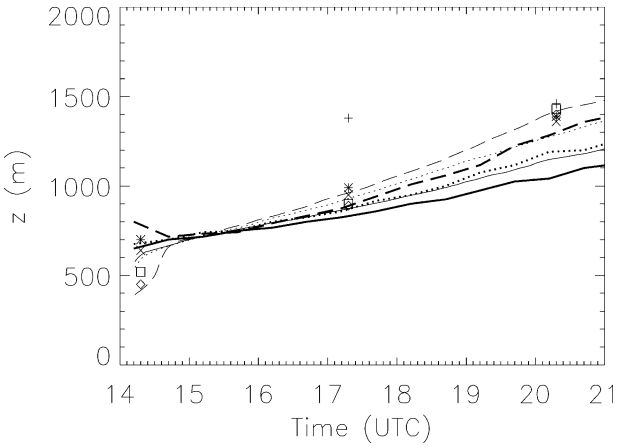

FIG. 9. MLD observed by the radiosondes launched at the different facilities—C1 (+), B1 (*), B4 (×), B5 (◇), and B6 (□)—and obtained by means of LES: B is a solid line, BG is a dotted line, and BGS is a dashed line. Thick lines represent h and thin lines h_s. The observed MLD for each observational site is estimated at the height at which the virtual potential temperature equals the virtual potential temperature of the mixed layer plus 1 K.

sidered in this section is based on a discontinuity at the interface, which is defined as a jump of the virtual potential temperature. In this kind of simple approach, referred to as zero-order jump model (Lilly 1968), the MLD is defined as the height of the minimum buoyancy flux. A more realistic approximation is based on the notion that the thickness of the inversion layer is finite and a linear variation of the potential temperature and buoyancy flux throughout the inversion layer exists (first-order jump model). In this model, the boundary layer depth is the height at which the buoyancy flux becomes zero (van Zanten et al. 1999). In their study, van Zanten et al. (1999) showed that for a cloud-free convective boundary layer the use of a first-order jump model concept to interpret the LES results gives a more complete physical interpretation of the entrainment flux. However, our parameterization is particularly designed to be used in coarse grid length models, such as a GCM. These models do not have enough vertical grid spacing or parameters to calculate the entrainment flux using a first-order jump model; for instance, they cannot calculate the evolution of the thickness of the interface.

a. Derivation

In this section, the value of $\beta = -\overline{w\theta_v}|_h/\overline{w\theta_v}|_0$ obtained from our LES runs is compared with previous parameterizations based on slab (zero-order jump) models. In spite of its simplicity, the proposed β formulation contains the most relevant processes that account for the entrainment in clear boundary layers. Notice that we take the role played by humidity into account by considering the buoyancy flux because it can lead to significant variations in the mixed-layer depth (Driedonks 1982b). We also assume that, although the surface heat fluxes evolve with time, this has little impact on the performance of the parameterization (Zilitinkevich 1991). We will verify this assumption a posteriori by comparing the results of the parameterization and the LES results.

To determine the role played by the various mechanisms that drive the entrainment flux, it is convenient to parameterize the terms of the TKE equation by means of scaling arguments (Tennekes and Driedonks 1981). Two main approaches can be followed with regard to the analysis and scaling of the various terms of the TKE budget. Equation (1) can be integrated over the mixed layer and then one can derive an expression for the entrainment flux based on scaling arguments. Alternatively, one can apply Eq. (1) directly at the entrainment interface. Similar expressions are found by using both approaches since similar scaling arguments are used to derive this expression (Driedonks 1982b). The parameterization presented here is based on the second approach.

We apply Eq. (1) at the inversion level ($z = h$). We assume that at this level mechanical energy produced at the interface is locally dissipated; that is, $D = S$. Figure 7a shows that this is a good approximation. Therefore, the only terms that remain at the TKE budget are, buoyancy, pressure, and transport, and in a steady-state situation the TKE budget reads $0 = B + P + T$. In consequence, one can close the entrainment flux as (Tennekes 1973, 1975)

$$-\frac{g}{\overline{\theta_v}}\overline{w\theta_v}|_h = C_F\frac{\sigma_w^3}{h}, \tag{3}$$

where the term on the right-hand side represents the contribution of the pressure and turbulent transport, h is the height of the minimum buoyancy flux, C_F is a constant, and σ_w is a turbulent velocity scale related to w_* and u_*. Following Driedonks (1982b), σ_w is defined as

$$\sigma_w^3 = w_*^3 + \frac{A}{C_F}u_*^3. \tag{4}$$

In previous experimental and theoretical work, different constants have been proposed for C_F and A. For a pure convective boundary layer, $u_* = 0$. Stull (1976a) summarized the available experimental data in pure convective conditions where C_F ranged from 0.1 to 0.5. As in previous studies (Tennekes 1973; Tennekes and Driedonks 1981; Driedonks 1982a,b), a value $C_F = 0.2$ is assumed here; this indicates that in pure convective conditions the entrainment flux is -20% of the surface buoyancy flux. This value has been widely observed (Stull 1988) and is frequently used in a GCM.

The value of A has been estimated for shear flows. In their laboratory experiments, Kato and Phillips (1969) found $A = 2.5$, but later Kantha et al. (1977) gave the value $A = 5$. Based on previous atmospheric boundary layer studies (Driedonks 1982b) and in our LES, we use a lower value of $A = 1.6$.

Substituting (4) into (3) and taking into account the definition of w_*, one can write the β ratio as

$$\beta = -\frac{\overline{w\theta_v}|_h}{\overline{w\theta_v}|_0} = C_F + A\left(\frac{u_*}{w_*}\right)^3, \tag{5}$$

which shows explicitly that the inclusion of surface wind shear increases the entrainment ratio. This effect can make the β parameter in a high wind situation twice as high as in a low wind situation (Betts and Ball 1994).

The parameterization (5) describes the entrainment ratio well, but it cannot deal with certain limiting cases. For instance, it is obvious that β must be reduced to zero when $d\theta_v/d_z = 0$ and $\Delta\theta_v = 0$, which is inconsistent with expression (5) where β is independent of $\Delta\theta_v$ and $d\theta_v/d_z$. Zilitinkevich (1975, 1991) pointed this out, and attributed the inconsistency to the omission of the temporal term (TE) in the parameterization of expression (1). He suggested that, when $d\theta_v/d_z$ and $\Delta\theta_v$ are small, the amount of TKE needed to spin up the entrained, nonturbulent fluid to the level of turbulence in the mixed layer [storage term TE in expression (1)] cannot be neglected with respect to the energy consumed to destroy buoyancy at the entrainment zone [term B in expression

(1)]. We have calculated this term TE in the budget equation of the TKE for the BGS simulation. Although the term is one order of magnitude smaller than the other terms, it is three orders of magnitude larger in the entrainment zone than in the bulk of the CBL. Therefore, it might contribute to modify the buoyancy flux at the interface. Furthermore, as it is discussed later, it can help to limit the calculation of unphysical values by the parameterization. This additional term could be closed by the following scaling expression:

$$\left(\frac{\partial \overline{e}}{\partial t}\right)_h = C_T \frac{\sigma_w^2}{h}\frac{dh}{dt}. \quad (6)$$

By using a zero-order jump model, and neglecting the subsidence velocity at $z = h$, the boundary layer growth (dh/dt) can be related to the strength of the capping inversion $\Delta\theta_v$ and to the buoyancy flux at $z = h$, as Lilly (1968) proposed,

$$\frac{dh}{dt} = -\frac{\overline{w\theta_v}|_h}{\Delta\theta_v}. \quad (7)$$

Substituting (7) into (6) and using (4), the TKE budget for this case TE = $B + P + T$ reads

$$\beta = -\frac{\overline{w\theta_v}|_h}{\overline{\overline{w\theta_v}|_0}} = \left[C_F + A\left(\frac{u_*}{w_*}\right)^3\right]\frac{1}{1 + C_T/\mathrm{Ri}_t}, \quad (8)$$

with a Richardson number (Ri_t) defined as

$$\mathrm{Ri}_t = \frac{gh}{\overline{\overline{\theta_v}}}\frac{\Delta\theta_v}{\sigma_w^2}, \quad (9)$$

which differs from Eq. (5) by the factor $(1 + C_T/\mathrm{Ri}_t)^{-1}$. According to (8), the expression (5) is valid asymptotically at sufficiently large values of $\Delta\theta_v$ and h. Moreover, (8) holds for the limiting case mentioned above. If $\Delta\theta_v \to 0$, the additional factor $(1 + C_T/\mathrm{Ri}_t)^{-1}$ tends to zero, and consequently, $\beta \to 0$. If one uses a value $C_T = 1.5$ (Driedonks 1982b), the inclusion of the storage term of the TKE equation modifies Eq. (5) by 5%.

We now turn our attention to the role of shear at the top of CBL. Stull (1976b, 1988) discussed the role of mechanical turbulence generated by wind shear at the surface and at the inversion level. He concluded that for winds roughly above 5 m s^{-1}, buoyancy is not the only factor that contributes to the development of the CBL. As is clear from Fig. 5, the observations show a large wind shear at the inversion, which is well reproduced by the BGS simulation. Furthermore, in this case, when large shear exists at the inversion, the mechanical turbulence produced is not totally locally dissipated, and the condition $D = S$ is not satisfied (see Fig. 7c).

It is therefore advisable to parameterize the contribution made to the TKE budget by the turbulence produced by local wind shear at the top of the mixed layer. In order to take this contribution into account, it is necessary to introduce into the parameterization (8) the shear production term (S) of the TKE budget equation (1). By using scaling arguments, one can include explicitly the shear at the inversion level as a function of the velocity jump.

The modified expression of the TKE budget, TE = $B + P + T + S$, reads (Tennekes and Driedonks 1981; Driedonks 1982b)

$$-\frac{gh}{\overline{\overline{\theta_v}}}\overline{w\theta_v}|_h = C_F\sigma_w^3 - C_T\sigma_w^2\frac{dh}{dt} + C_M(\Delta V_e)^2\frac{dh}{dt}, \quad (10)$$

where ΔV_e is the modulus of the velocity jump ΔU and ΔV at the inversion base, and C_M is a constant. As Driedonks (1982b) suggested, in this case

$$\sigma_w^3 = w_*^3 + \eta^3 u_*^3, \quad (11)$$

with $\eta = 2$, where $\eta^3 = A/C_F$. In our simulations, at 1730 and 2030 UTC, we have obtained σ_w values equal to 1.74 and 1.87 m s^{-1}, in close agreement with the observed values 1.82 and 1.97 m s^{-1} respectively.

Using (7) to close the boundary layer growth (dh/dt), Eq. (10) can be written as

$$\beta = -\frac{\overline{w\theta_v}|_h}{\overline{\overline{w\theta_v}|_0}} = C_F\left[1 + \eta^3\left(\frac{u_*}{w_*}\right)^3\right]\frac{1}{1 + C_T/\mathrm{Ri}_t - C_M/\mathrm{Ri}_{\mathrm{GS}}}, \quad (12)$$

with a Richardson number ($\mathrm{Ri}_{\mathrm{GS}}$) defined as

$$\mathrm{Ri}_{\mathrm{GS}} = \frac{gh}{\overline{\overline{\theta_v}}}\frac{\Delta\theta_v}{(\Delta V_e)^2}. \quad (13)$$

b. Limiting values and selection of constants

It is important to analyze briefly the possible extreme values (range of applicability) and to comment on the selection of the most optimal constants for Eq. (12).

From observations, Price et al. (1978) estimated $C_M \approx 0.7$. To estimate the two bulk Richardson numbers Ri_t (9) and $\mathrm{Ri}_{\mathrm{GS}}$ (13), the temperature jump is calculated as $\Delta\theta_v = \theta_v|_{n_i} - \theta_v|_{10}$, where $\theta_v|_i$ is the value of the virtual potential temperature at level i, $\theta_v|_{10}$ is considered to be the reference virtual potential temperature $\overline{\overline{\theta_v}}$, and n_i is a time-dependent level just above the inversion. The same procedure is used to calculate the velocity jumps. Due to the well-mixed layer reproduced by the simulations, there is no difference in the calculation of the jumps if other levels different than 10, within the mixed layer, are considered. Above the boundary layer the situation is more sensitive to the growth of the inversion. For the calculation of n_i, levels close to the top limit of the entrainment zone have to be used for obtaining a realistic value of the jump. For this reason, a temporal evolution of this level is taken into account in the calculation of Ri_t and $\mathrm{Ri}_{\mathrm{GS}}$.

Although Driedonks (1982b) suggested using $C_F = 0.6$ in the TKE budget parameterization if shear at the inversion is considered, $C_F = 0.2$ is retained in order

TABLE 2. The TKE terms (B: buoyancy, P: pressure transport, S: shear production at the inversion, T: turbulent transport, TE: tendency) and the constants of expression (12) used for each of the comparisons.

	$B + P + T$ ($\eta = 2$, $C_F = 0.2$)	TE ($C_T = 4$)	S ($C_M = 0.7$)
B	Yes ($u_* = 0$)	Yes	No ($\Delta V_e = 0$)
BG	Yes	Yes	No ($\Delta V_e = 0$)
BGS	Yes	Yes	Yes

to maintain consistency with the situation in a convective boundary layer driven only by buoyancy. So doing, the original Tennekes–Zilitinkevich model [Eq. (8)] is retrieved when $\Delta V_e = 0$, that is, absence of shear at the interface. Moreover, it is clear that Eq. (12) is equivalent to Eq. (5) in the limit of sufficiently large values of $\Delta\theta_v$ or h; that is, $1 \gg C_T/\mathrm{Ri}_t - C_M/\mathrm{Ri}_{\mathrm{GS}}$.

LES results for the central part of the day (from 1600 UTC to 2000 UTC) produce $\mathrm{Ri}_{\mathrm{GS}} \in [6, 1.5]$. If $C_T = 0$, the factor $1/(1 - C_M/\mathrm{Ri}_{\mathrm{GS}})$ can modify the entrainment coefficient by a factor ranging from 1.13 to 1.87. The only physical mechanism that can balance this tendency to very large or negative values is the temporal term [see expressions (1) and (12)]. Supposing $C_T = 1.5$, as Driedonks (1982b) suggested, too-high values of β are obtained with expression (12) for the BGS case. In order to prevent these high values of β, and following André et al. (1978), $C_T = 4$ is proposed and used in expression (12).

Due to the different sign of the term with Ri_t and the term with $\mathrm{Ri}_{\mathrm{GS}}$ in the denominator of expression (12), it is important to study the possible asymptotic behavior. The denominator vanishes for the case

$$C_M(\Delta V_e)^2 - C_T\sigma_w^2 = \frac{gh\Delta\theta_v}{\overline{\theta_v}}. \qquad (14)$$

Typical values during convective diurnal situation of $gh\Delta\theta_v/\overline{\theta_v}$ ranged from 100 to 150 $\mathrm{m^2\ s^{-2}}$. With the prescribed values of C_M and C_T, this situation is only obtained with very high values of the velocity jumps at the interface ($\Delta V_e > 12\ \mathrm{m\ s^{-1}}$) and very weak convective situations. In our studied boundary layer, the term on the left-hand side of expression (14) approximately ranges from 80 to 100 $\mathrm{m^2\ s^{-2}}$, and the term on the right-hand side is always smaller than the left-hand side term, reaching a maximum value of 60 $\mathrm{m^2\ s^{-2}}$ at the end of the simulation, when the turbulence generated by convection is much lower than the mechanical turbulence.

c. Evaluation

The final parameterization of β [expression (12)] is compared with the values obtained directly with the B, BG, and BGS simulations. The output of the B, BG, or BGS simulations is used as input to calculate u_*, w_*, Ri_t, and $\mathrm{Ri}_{\mathrm{GS}}$ in the parameterization (12). Table 2 shows the different TKE terms and its respective constants used in the parameterization (12) to compare with the LES results B, BG, and BGS.

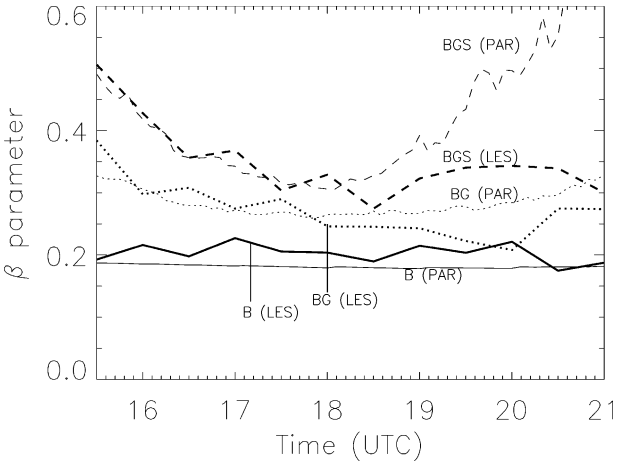

FIG. 10. Time evolution of the β parameter averaged every 30 min for the various LES runs (thick lines, LES) and represented by expression (12) (thin lines, PAR): B (solid line), BG (dotted line), and BGS (dashed line). The values of C_F, η, C_T, and C_M in expression (12) for each of the comparisons are listed in Table 2.

Figure 10 shows, for all three simulations, the β evolution during the initial and central parts of the day, when convection is the dominant process driving the turbulence. After 2100 UTC, the initial sensible heat flux has decreased in value by 50% with respect its maximum value (see Fig. 3c), and thereafter, a regime of decaying turbulence is established (Nieuwstadt and Brost 1986). It is clear from Fig. 10 that, in general, wind shear in the boundary layer increases the entrainment coefficient β with respect to the pure buoyancy case. Specifically, by comparing β for the BG and BGS simulations one finds that, if the shear is not only at the surface (BG simulation) but also at the inversion level (BGS simulation), the entrainment coefficient is increased. Since, as mechanical production of turbulence can also contribute to entrainment, β varies in a sheared boundary layer during the diurnal cycle as the relative amounts of buoyant and mechanical production change (Stull 1976b, 1988). This figure also shows the evolution of β calculated from the expression (12) with the parameters shown in Table 2. A constant value $\beta \approx 0.2$ predicts fairly accurately the evolution of the entrainment ratio for the B simulation. Moreover, the BG parameterization agrees very well with the BG simulation for the entire period studied. For the BGS simulation, the parameterization is in close agreement with the LES results obtained during the growth and maintenance of the CBL (first 4h). At the end of day, when turbulence generated by convection decays, LES cannot reproduce the conditions in which the boundary layer collapses: w_*, h, and $\Delta\theta_v$ decreased, and ΔV_e increased. As a result, C_T/Ri_t calculated from LES can-

TABLE 3. Mean value (averaged between 1530 UTC and 2100 UTC) of the β parameter and entrainment ratio for LES results and for the parameterization [Eqs. (12) and (13), respectively].

	B	BG	BGS
β			
LES	0.20	0.25	0.33
Parameterization	0.18	0.28	0.41
E			
LES	0.013	0.022	0.028
Parameterization	0.005	0.010	0.018

not balance $C_M/\mathrm{Ri}_{\mathrm{GS}}$ at the end of the day, and the factor $1/(1 + C_T/\mathrm{Ri}_t - C_M/\mathrm{Ri}_{\mathrm{GS}})$ increases in value. Therefore, the large values of the BGS parameterization shown in Fig. 10 can be explained in terms of the nonphysical values given by the LES in the regime of decaying turbulence. It should be noted that the parameterization (12) is designed mainly to represent the growth and maintenance of the CBL.

The evolution of the convective boundary layer can be also studied by calculating the entrainment rate, $E \propto dh/dt$ (Zilitinkevich 1991). In our case, we have defined

$$E = \frac{\sigma_w^2}{w_*^3}\frac{dh}{dt}, \tag{15}$$

in order to introduce the two convective velocities used in our study. Using Eqs. (7) and (10) and the definition of β (12), the entrainment rate can be written in a simple way as

$$E = \frac{\beta}{\mathrm{Ri}_t}. \tag{16}$$

Taking into account the definition of σ_w (11), this expression follows the power law $E \propto \mathrm{Ri}^{-1}$.

Table 3 shows the mean values of the β parameter and entrainment rate E between 150 and 480 min of simulation (between 1530 UTC and 2100 UTC) for the various LES runs and for the parameterizations. With regard to the β comparison, as can be observed, the parameterization (12) reproduces quite well the mean values obtained with LES runs for the three simulations performed. As a comparison, Betts and Ball (1994) obtained from observations similar values to those in the BGS case ($\beta = 0.44 \pm 0.21$). The entrainment rate calculated by the parameterization underestimates the entrainment values obtained by LES. However, although there are some reservations about the use of this type of formulation with surface heat fluxes that evolve with time (Zilitinkevich 1991), the results shown in Table 3 and Fig. 10 lead us to propose expression (12) to calculate the buoyancy entrainment flux in large atmospheric models.

5. Summary and conclusions

The influence of shear on the entrainment fluxes was studied by means of large eddy simulations and observations. The results discussed in this paper show that LES can be used to describe the growth and maintenance of the boundary layer under realistic conditions. Using the data obtained at the SGP ARM site on 20 June 1997 as initial vertical profiles for the potential temperature, specific humidity, and geostrophic winds, we simulated the evolution of the boundary layer during 11 h, and we compared the vertical profiles and mixed-layer depth with the observations; the comparison yielded good agreement. However, our main purpose was to deepen our understanding of the role of shear in the entrainment processes. Therefore, we performed two additional simulations, one without shear and one with shear only at the surface. As previous studies found, our results have shown that the presence of horizontal geostrophic winds in convective situations enhances the entrainment flux and modifies the convection pattern. The entrainment flux can increase still more if shear is present not only at the surface but also in the inversion zone. The larger entrainment fluxes generated in the BGS simulation produce a boundary layer that is warmer and drier than the one observed in the B and BG cases. As a consequence, the values for the mixed-layer depth obtained for the BGS simulation are higher than the values obtained in the B and BG simulations.

By means of the LES, it is possible to obtain the various contributions to the TKE budget. Consequently, the influence of shear at the inversion is clearly shown in the vertical distribution of the various terms of the TKE budget. The TKE budget in the BGS simulation shows that the shear term is the largest term in the entrainment zone, and it is therefore necessary to take it into account in the parameterization of the TKE budget. The profiles of the buoyancy heat flux corroborate this result, showing an enhancement of the entrainment flux and, consequently, a larger increase in the depth of the boundary layer.

These results are used to refine and verify a parameterization of the entrainment flux that can be implemented in general circulation models. By comparing previous zero-order jump parameterizations of the entrainment flux used in large-scale models with the LES results, we obtain a simple expression for the ratio of entrainment flux to the surface flux β. The parameterization fulfills the following properties. First, in the pure buoyancy case, the standard value $\beta = 0.2$, which includes the buoyancy, transport, and pressure contributions, aptly describes the evolution of the entrainment ratio. Second, if the temporal term of the TKE budget is considered, in the absence of a clear potential temperature jump, or for a very small temperature lapse rate, the ratio β becomes zero. Third, the inclusion of the shear contribution in the TKE budget [see the pro-

posed parameterization (12) and its respective constants] allows us to introduce into the β ratio the significant contribution made by the shear at the surface and at the inversion level. During the initial and central parts of the day, before the turbulence generated by convection started to decay, the values for the entrainment rates obtained with LES and with the proposed parameterization are in close agreement. The LES results indicate that the β ratio increases its value compared to the pure buoyancy case due to the surface shear ($\beta = 0.25$) and combined surface and geostrophic shear ($\beta = 0.33$). Regarding the parameterizations, slightly higher values with respect to the LES results are found for the shear cases, giving an average value of $\beta = 0.28$ when the initial vertical wind profile reproduces the shear at the surface and a value of $\beta = 0.41$ when wind shear is present at the surface and at the top of the CBL.

Acknowledgments. The data used in this paper were obtained from the Atmospheric Radiation Measurement (ARM) Program sponsored by the U.S. Department of Energy. We are particularly grateful to Thomas Ackerman, David Cook, Mark Miller, and Ping Zhu for supplying and interpreting the data. We thank Mandy Khaiyer of AS&M, Inc., Hampton, Virginia, for providing the GOES imagery. Discussions with Harm Jonker are greatly appreciated. The comments of the referees are also acknowledged. D. Pino was partially supported by the project IMMPACTE (CIRIT, DMA, Barcelona, Spain). The visits by the first author to the IMAU were partially supported by the EU program EUROCS (European Project on Cloud Systems in Climate Models). The resources of CESCA and CEPBA were used for parts of the work.

Dr. P. G. Duynkerke died suddenly during the last stage of the research and will be sorely missed.

REFERENCES

André, J. C., G. De Moor, P. Lacarrère, G. Therry, and R. du Vachat, 1978: Modeling the 24-hour evolution of the mean and turbulent structure of the planetary boundary layer. *J. Atmos. Sci.,* **35,** 1861–1883.

Artaz, M. A., and J. C. André, 1980: Similarity studies of entrainment in convective mixed layers. *Bound.-Layer Meteor.,* **19,** 51–66.

Arya, S. P. S., and J. C. Wyngaard, 1975: Effect of baroclinicity on wind profiles and the geostrophic drag law for the convective planetary boundary layer. *J. Atmos. Sci.,* **32,** 767–778.

Barr, S., and D. L. Sisterson, cited 2000: Local analysis report for the Southern Great Plains. [Available online at http://www.arm.gov/docs/documents/site_reports/index.html.]

Betts, A. K., 1973: Non-precipitating cumulus convection and its parameterization. *Quart. J. Roy. Meteor. Soc.,* **99,** 178–196.

——, and J. H. Ball, 1994: Budget analysis of FIFE 1987 sonde data. *J. Geophys. Res.,* **99,** 3655–3666.

Bretherton, C. S., and Coauthors, 1999: An intercomparison of radiatively driven entrainment and turbulence in a smoke cloud, as simulated by different numerical models. *Quart. J. Roy. Meteor. Soc.,* **125,** 391–423.

Carson, D. J., 1973: The development of a dry inversion-capped convectively unstable boundary layer. *Quart. J. Roy. Meteor. Soc.,* **99,** 450–467.

Christian, T. W., and R. M. Wakimoto, 1989: The relationship between radar reflectivities and clouds associated with horizontal roll convection on 8 August 1982. *Mon. Wea. Rev.,* **117,** 1530–1544.

Cuijpers, J. W. M., and P. G. Duynkerke, 1993: Large eddy simulation of trade wind cumulus clouds. *J. Atmos. Sci.,* **50,** 3894–3908.

——, and A. A. M. Holtslag, 1998: Impact of skewness and nonlocal effect on scalar and buoyancy fluxes in convective boundary layers. *J. Atmos. Sci.,* **55,** 151–162.

Culf, A. D., 1992: An application of simple models to Sahelian convective boundary-layer growth. *Bound.-Layer Meteor.,* **58,** 1–18.

Driedonks, A. G. M., 1982a: Sensitivity analysis of the equations for a convective mixed layer. *Bound.-Layer Meteor.,* **22,** 475–480.

——, 1982b: Models and observations of the growth of the atmospheric boundary layer. *Bound.-Layer Meteor.,* **23,** 283–306.

——, and H. Tennekes, 1984: Entrainment effects in the well-mixed atmospheric boundary layer. *Bound.-Layer Meteor.,* **30,** 75–105.

Dubosclard, G., 1980: A comparison between observed and predicted values for the entrainment coefficient in the planetary boundary layer. *Bound.-Layer Meteor.,* **18,** 473–483.

Dudhia, J., 1993: A nonhydrostatic version of the Penn State–NCAR mesoscale model: Validation tests and simulation of an Atlantic cyclone and cold front. *Mon. Wea. Rev.,* **121,** 1493–1513.

Fairall, C. W., 1984: Wind shear enhancement of entrainment and refractive index structure parameter at the top of a turbulent mixed layer. *J. Atmos. Sci.,* **41,** 3472–3484.

Fedorovich, E., 1995: Modeling the atmospheric convective boundary layer within a zero-order jump approach: An extended theoretical framework. *J. Appl. Meteor.,* **34,** 1916–1928.

——, F. T. M. Nieuwstadt, and R. Kaiser, 2001a: Numerical and laboratory study of a horizontally evolving convective boundary layer. Part I: Transition regimes and development of the mixed layer. *J. Atmos. Sci.,* **58,** 70–86.

——, ——, and ——, 2001b: Numerical and laboratory study of a horizontally evolving convective boundary layer. Part II: Effects of elevated wind shear and surface roughness. *J. Atmos. Sci.,* **58,** 546–560.

Garratt, J. R., 1992: *The Atmospheric Boundary Layer*. Cambridge University Press, 316 pp.

Kantha, L. H., O. M. Phillips, and R. S. Azad, 1977: On turbulent entrainment at a stable density interface. *J. Fluid Mech.,* **79,** 753–768.

Kato, H., and O. M. Phillips, 1969: On the penetration of a turbulent layer into stratified fluid. *J. Fluid Mech.,* **37,** 643–655.

Khanna, S., and J. G. Brasseur, 1998: Three-dimensional buoyancy and shear-induced local structure of the atmospheric boundary layer. *J. Atmos. Sci.,* **55,** 710–743.

LeMone, M. A., 1973: The structure and dynamics of horizontal roll vortices in the planetary boundary layer. *J. Atmos. Sci.,* **30,** 1077–1091.

Lilly, D. K., 1968: Models of cloud-topped mixed layer under a strong inversion. *Quart. J. Roy. Meteor. Soc.,* **94,** 292–309.

Moeng, C.-H., and P. P. Sullivan, 1994: A comparison of shear- and buoyancy-driven planetary boundary layer flows. *J. Atmos. Sci.,* **51,** 999–1022.

Nieuwstadt, F. T. M., and R. A. Brost, 1986: The decay of convective turbulence. *J. Atmos. Sci.,* **43,** 532–546.

Price, J. F., C. N. K. Mooers, and J. C. van Leer, 1978: Observation and simulation of storm-induced mixed layer deepening. *J. Phys. Oceanogr.,* **8,** 582–599.

Schmidt, H., and U. Schumann, 1989: Coherent structure of the convective boundary layer derived from large-eddy simulations. *J. Fluid Mech.,* **200,** 511–562.

Sorbjan, Z., 2001: An evaluation of local similarity at the top of the mixed layer based on large-eddy simulations. *Bound.-Layer Meteor.,* **101,** 183–207.

Stull, R. B., 1976a: The energetics of entrainment across a density interface. *J. Atmos. Sci.,* **33,** 1260–1267.

——, 1976b: Mixed-layer depth model based on turbulent energetics. *J. Atmos. Sci.,* **33,** 1268–1278.
——, 1988: *An Introduction to Boundary Layer Meteorology*. Kluwer Academic Press, 670 pp.
Sykes, R. I., and D. S. Henn, 1989: Large-eddy simulation of turbulent sheared convection. *J. Atmos. Sci.,* **46,** 1106–1118.
Tennekes, H., 1973: A model for the dynamics of the inversion above a convective boundary layer. *J. Atmos. Sci.,* **30,** 558–567.
——, 1975: Reply. *J. Atmos. Sci.,* **32,** 992–995.
——, and A. G. M. Driedonks, 1981: Basic entrainment equations for the atmospheric boundary layer. *Bound.-Layer Meteor.*, **20,** 515–531.
van Zanten, M. C., P. G. Duynkerke, and J. W. M. Cuijpers, 1999: Entrainment parameterization in convective boundary layers. *J. Atmos. Sci.,* **56,** 813–828.
Zeman, O., and H. Tennekes, 1977: Parameterization of the turbulent energy budget at the top of the daytime atmospheric boundary layer. *J. Atmos. Sci.,* **34,** 111–123.
Zilitinkevich, S. S., 1975: Comments on ''A model for the dynamics of the inversion above a convective boundary layer.'' *J. Atmos. Sci.,* **32,** 991–992.
——, 1991: *Turbulent Penetrative Convection.* Avebury Technical, 180 pp.